

# High power single-sided Bragg reflection waveguide lasers with dual-lobed far field

L.J. Wang · Y. Yang · Y.G. Zeng · L.J. Wang ·  
C.Z. Tong · X.N. Shan · H.X. Zhao · R. Wang · S.F. Yoon

Received: 27 September 2011 / Revised version: 28 March 2012 / Published online: 24 May 2012  
© Springer-Verlag 2012

**Abstract** We report on 980-nm InGaAs/GaAs lasers with dual-lobed far field based on a single-sided Bragg reflection waveguide (BRW). The high slope efficiency  $\sim 0.92$  W/A and a continuous wave (CW) output power  $> 1.5$  W (3.2 W pulsed) have been obtained. The threshold current density is as low as  $253$  A/cm<sup>2</sup> for a 1.5-mm-long device and the transparency current density is only  $140$  A/cm<sup>2</sup>. The further analysis shows the intrinsic reason for the single-lobed or the dual-lobed far-field distribution is determined by the mode shape in the cavity, not the single-sided or dual-sided BRW structure. The condition to achieve a narrow single-lobed far-field distribution is discussed.

## 1 Introduction

The output power of diode lasers has been driven to higher and higher values in the past few years [1, 2]. One important approach lies in expanding the waveguide thickness in the transverse direction (vertical direction) [3]. This large optical cavities (LOC) laser structure leads to reduced optical

power density on the laser facets, resulting in increased output power limited by catastrophic optical damage (COD). However, this method suffered from higher-order transverse modes operation and the decrease of modal gain when simply increasing the waveguide thickness [4]. In order to overcome this problem, Bragg reflection waveguide (BRW) was incorporated in the laser transverse epi-design [5], which use distributed reflection within the periodic Bragg reflectors rather than traditional total internal reflection (TIR) to confine light. The BRW lasers (BRLs) can be designed to have large mode volumes with significant mode discrimination [5, 6], allowing for stable, single transverse mode operation even at high output power.

In recent years, both the single-sided and dual-sided BRLs have made great progress. The single-sided BRLs or the so-called longitudinal photonic bandgap crystal (PBC) lasers demonstrate the ultra-narrow vertical beam divergence of about  $5\text{--}8^\circ$  [7–9], which are promising for the application of high-brightness lasers. The dual-sided BRLs demonstrate the low threshold ( $\sim 157$  A/cm<sup>2</sup>) [10] and high temperature stability [11] with two separated lobes in the vertical far field (FF), which are favored for the phase-matched nonlinear BRW [12, 13]. The compatibility of BRLs with the nonlinear BRWs provides the potential possibility to develop monolithic integration, electrically injected, and highly efficient nonlinear frequency conversion sources [10].

However, it is inscrutable on the FF behavior of BRLs. The dual-lobed or multi-lobed FF patterns were thought as the nature of dual-sided BRL, and attributed to the dual-sided transverse Bragg resonance based on the quarter-wave (QtW) Bragg condition [14]. On the contrary, the narrow single-lobed FF patterns were considered as the unique advantage of single-sided BRLs [7–9, 14]. It seems that the lobe characteristic of FF is determined by the single-sided

---

L.J. Wang · Y. Yang · Y.G. Zeng · L.J. Wang · C.Z. Tong (✉) ·  
X.N. Shan

Key laboratory of Excited State Processes, Changchun Institute of Optics, Fine Mechanics and Physics, Chinese Academy of Sciences, Changchun 130033, China  
e-mail: [tongcz@ciomp.ac.cn](mailto:tongcz@ciomp.ac.cn)  
Fax: +86-0431-86176348

L.J. Wang  
Graduate School of the Chinese Academy of Sciences, Beijing  
100049, China

H.X. Zhao · R. Wang · S.F. Yoon  
School of Electrical and Electronic Engineering, Nanyang Technological University, Singapore 639798, Republic of Singapore

or dual-sided BRW structure. However, in this letter, we demonstrate the dual-lobed FF can also be achieved in the single-sided BRLs. The high output power and low threshold current were demonstrated. The reason to form the single lobe or dual lobes in the FF distribution is discussed.

## 2 Device design and fabrication process

The designed single-sided BRL consists of a low index optical defect layer, bottom Bragg reflector and top cladding layer. Figure 1(a) shows the refractive index profile of designed single-sided BRL. The bottom Bragg reflector is eight pairs of n-doped  $\text{Al}_{0.1}\text{Ga}_{0.9}\text{As}/\text{Al}_{0.3}\text{Ga}_{0.7}\text{As}$ , whose thickness is 100 nm and 750 nm, respectively. The gain material is two 6-nm  $\text{In}_{0.2}\text{Ga}_{0.8}\text{As}$  quantum wells (QWs) separated by 10-nm GaAs barrier, which is sandwiched between the optical defect layer and the 1.4- $\mu\text{m}$ -thick p-doped  $\text{Al}_{0.35}\text{Ga}_{0.65}\text{As}$  cladding layer. The total thickness of the BRL was 9.83  $\mu\text{m}$ . All interfaces were linearly graded in composition over 20 nm to reduce the electrical resistance of device.

A numerical calculation of near field distribution of fundamental mode is shown in Fig. 1(b). In the calculations, the refractive index of  $\text{In}_{0.2}\text{Ga}_{0.8}\text{As}$  was selected as 3.65 at the 980 nm wavelength [15], and the refractive indices of the AlGaAs materials at room temperature (RT) were taken from Ref. [16]. As can be seen, the transverse modal size is enlarged significantly due to the extension of the optical field throughout the entire width of the Bragg reflector regions.

The laser wafer was grown on a Si-doped GaAs (100)-oriented substrate by an Aixtron-200 MOCVD system. The group III sources are trimethylgallium (TMGa), TMAI and TMIIn with  $\text{H}_2$  as the carrier gas, and the group V source is  $\text{AsH}_3$ . The p-type dopant is Zn, and the n-type dopant is Si. The growth temperature is 710  $^\circ\text{C}$  for all layers except for the InGaAs QWs, which is 650  $^\circ\text{C}$ .

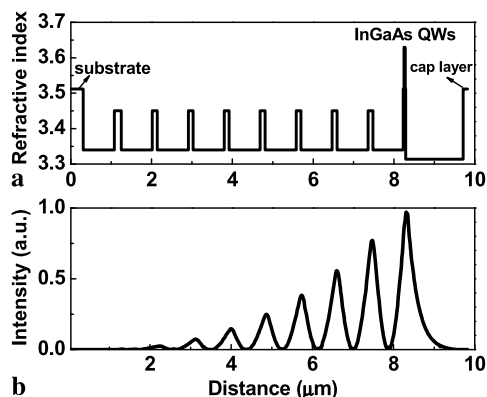


**Fig. 1** (a) Refractive index profile and (b) electric field distribution of fundamental mode in the BRL

After wafer growth, a 50- $\mu\text{m}$ -wide mesa was formed by photolithography and wet chemical etching through the  $\text{p}^+$ -GaAs cap layer and down to partial p-cladding layer. The etching depth was 1.1  $\mu\text{m}$ . Then 300-nm  $\text{SiO}_2$  electrical insulating layer was deposited and contact window opening was done by normal photolithography and wet etching. After backside thinning and polishing, Ti-Pt-Au and AuGeNi-Au contact were, respectively, evaporated on the p- and n-side. The wafer was then cleaved into individual laser diodes in various cavity lengths. For the experimental characterization, the individual laser chips were mounted epi-side down on a copper heat-sink using indium solder without facet passivation or coating.

## 3 Results and discussion

The fabricated laser diodes were measured under continuous wave (CW) and pulsed operation (pulse width = 50  $\mu\text{s}$ , repetition rate = 100 Hz) at RT.

### 3.1 Light-current-voltage characteristics

Figure 2 depicts the pulsed and CW light-current-voltage (L-I-V) characteristics of an uncoated 50- $\mu\text{m}$ -wide, 800- $\mu\text{m}$ -long laser. In the CW operation, the threshold current is 110 mA, corresponding to a threshold current density  $J_{\text{th}}$  of 275  $\text{A}/\text{cm}^2$ , and the CW output power exceeds 1.5 W from two facets, which is limited by the current source. The slope efficiency was 0.92 W/A and the wall-plug efficiency was 48 % at 1 A current in CW regime (both facets). No COD was observed at the uncoated BRL laser in the pulse operation. The highest output power in the pulse operation is about 3.2 W, which is limited by the thermal rollover due to the poor heat dissipation in our measurement system. The threshold voltage is about 1.5 V.

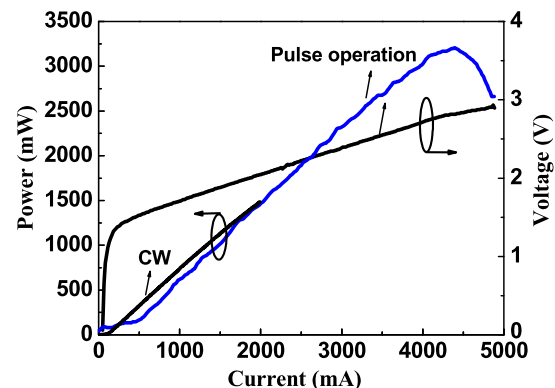


**Fig. 2** CW and pulsed light-current-voltage (L-I-V) characteristics of an uncoated single-sided BRL (both facets)

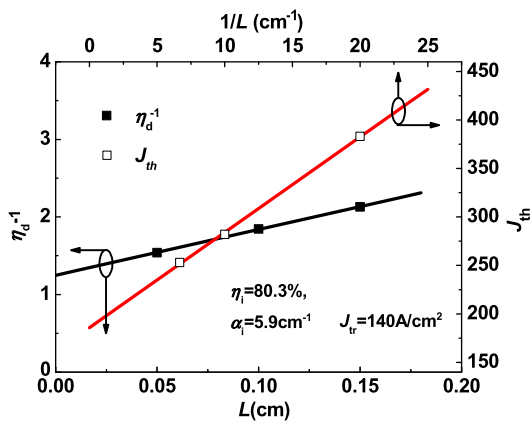


**Fig. 3** Inverse external quantum efficiency ( $\eta_d^{-1}$ ) as a function of cavity length  $L$  (solid squares) and  $J_{th}$  as a function of inverse cavity length  $1/L$  (hollow squares). The solid lines are the simulated results

### 3.2 Loss and transparency current density

To get the loss and transparency current of this single-sided BRL, the simulation was done as follows. The inverse external quantum efficiency as a function of cavity length  $L$  at RT is shown in Fig. 3 as solid squares. The internal quantum efficiency ( $\eta_i$ ) and internal loss values ( $\alpha_i$ ) could be acquired from the following equation:

$$\eta_d^{-1} = \eta_i^{-1} \left( \frac{\alpha_i}{\ln(1/R)} L + 1 \right) \tag{1}$$

where  $L$  is the cavity length.  $R = [(n_{\text{eff}} - 1)/(n_{\text{eff}} + 1)]^2$ , is the reflectivity of the cleaved facets. For our devices, the effective refractive index  $n_{\text{eff}}$  of fundamental mode is 3.285, so  $R$  is about 0.284. From Fig. 3, we find that the internal quantum efficiency ( $\eta_i$ ) is about 80.3 %, and the internal loss  $\alpha_i \sim 5.9 \text{ cm}^{-1}$ .

The transparency current density ( $J_{tr}$ ) can be calculated using the following formula [17]:

$$J_{th} = J_{tr} + \frac{\alpha_i}{g_0 \Gamma} + \frac{1}{L} \frac{1}{g_0 \Gamma} \ln(1/R) \tag{2}$$

where  $\Gamma$  is the optical confinement factor and  $g_0$  is the material gain parameter. The  $J_{th}$  as function of inverse cavity length are shown in Fig. 3 as hollow squares. From that the transparency current density ( $J_{tr}$ ) can be calculated to be 140 A/cm<sup>2</sup>. As shown in Fig. 3, the threshold current density  $J_{th}$  is as low as 253 A/cm<sup>2</sup> for 1.5-mm-long devices.

### 3.3 Far-field behavior

The measured FF distributions in the vertical direction are shown in Fig. 4(a). The most prominent feature is that the FF shows two pronounced lobes symmetrically located at  $\pm 32^\circ$  in the vertical direction, being in good agreement with the calculated results shown in Fig. 4(b). The full width at half maximum (FWHM) of one lobe is about  $11.6^\circ$ .

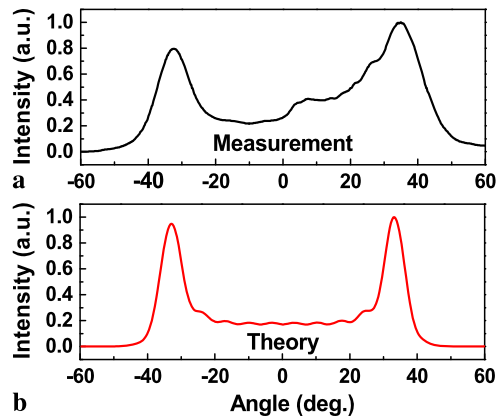


**Fig. 4** (a) Measured and (b) calculated far-field distribution of the BRL in the vertical direction

Note that the structure of single-sided BRL studied here is very similar with that reported in Ref. [8], however, the FF of the BRL in Ref. [8] shows a narrow single lobe. To clarify the backside intrinsic mechanism, more analysis is necessary. From the Rayleigh-Sommerfeld diffraction integral [18], we can get the intensity of FF distribution:

$$I_{FF} \propto \left| \cos \theta \int_{-\infty}^{+\infty} \Phi(x) \exp(-ik_0 x \sin \theta) dx \right|^2 \tag{3}$$

where  $\Phi(x) = \exp[-(\frac{x}{w})^2]$ , describe the optical intensity distribution or the mode shape in the laser cavity.  $x$  is the coordinate of cavity, and  $\theta$  is the FF angle.

If the mode shape is the Gaussian or an attenuated wave like Shape I shown in Fig. 5(a), the FF distribution obtained from Eq. (3) will be single lobe, and the FWHM becomes narrow with the increase in the distribution width  $w$ . As can be seen in Fig. 5(b), the FF angle can be less than  $3^\circ$  if the distribution size of modes can be extended to above 14  $\mu\text{m}$ . As to the TIR laser, in general, the distribution size of optical field is below 2  $\mu\text{m}$  due to the quickly attenuated optical field in the low index cladding layer, which is the reason why the TIR laser shows the large FF angle above  $30^\circ$ . Ref. [8] experimentally demonstrated the narrow FF distribution with FWHM as narrow as  $5^\circ$  by 16.5- $\mu\text{m}$ -thick Bragg reflector with a mode shape of Shape I, the similar results can also be found in Refs. [7] and [9].

However, if the mode shape follows Shape II, i.e. there exist periodic points corresponding to the optical intensity equal zero, and the calculation of FF distribution will have to follow the theory presented in Ref. [19]. In this case, the central portion of the field profile in the Bragg mirrors can be expressed as a cosine function with a half-period. The FF distribution will come with a dual-lobe as shown in Ref. [19]. Therefore, single-lobed or dual-lobed FF is determined intrinsically by the mode shape, not the single-sided or dual-sided BRW structures.

In our designed single-sided BRL, the near field distribution of fundamental mode follows the Shape II as shown in

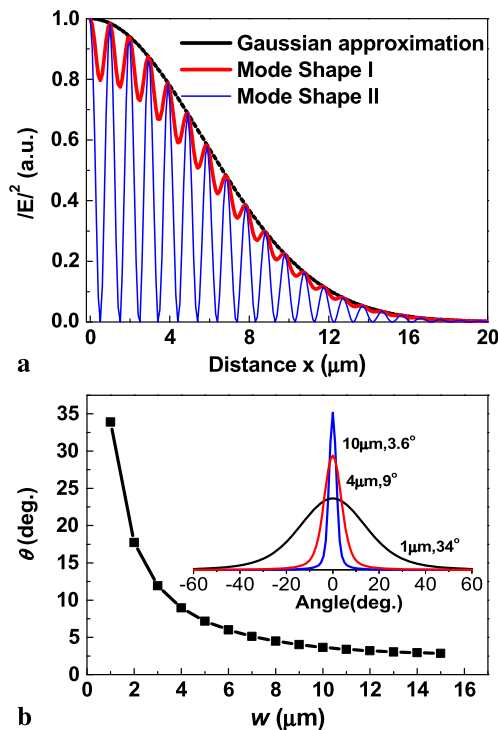


**Fig. 5** (a) Three mode shapes of near field distribution, Gaussian approximation (*dot*), Shape I (*thick line*), and Shape II (*thin line*); (b) Far-field FWHM as a function of mode distribution width  $w$ , *top inset* shows three examples

Fig. 1(b), so our devices present a two symmetric lobes in the experimentally measured FF.

#### 4 Conclusion

In summary, we have demonstrated the dual-lobed FF of a laser based on a single-sided BRW. We find the intrinsic reason to determine the single-lobed or dual-lobed characteristics of FF is the mode shape confined in the cavity. The high output power and low threshold current density and transparency current density are achieved. We believe these results will contribute to the development of high performance BRLs.

**Acknowledgements** We acknowledge the financial support from the National Natural Science Foundation of China under Grant No. 61076064 and the Hundred Talents Program of Chinese Academy of Sciences.

#### References

1. V.V. Bezotosnyi, V.Yu. Bondarev, O.N. Krokhin, G.T. Mikaelyan, V.A. Oleshchenko, V.F. Pevtsov, Yu.M. Popov, E.A. Cheshev, *Quantum Electron.* **39**, 241 (2009)
2. P. Crump, G. Blume, K. Paschke, R. Staske, A. Pietrzak, U. Zeimer, S. Einfeldt, A. Ginolas, *Proc. SPIE* **7198**, 719814 (2009)
3. L.J. Mawst, A. Bhattacharya, J. Lopez, D. Botez, D.Z. Garbuzov, L. DeMarco, J.C. Connolly, M. Jansen, F. Fang, R.F. Nabiev, *Appl. Phys. Lett.* **69**, 1532 (1996)
4. A. Pietrzak, H. Wenzel, G. Erbert, G. Tränkle, *Opt. Lett.* **33**, 2188 (2008)
5. N.N. Ledentsov, V.A. Shchukin, *Opt. Eng.* **41**, 3193 (2002)
6. B.R. West, A.S. Helmy, *J. Opt. Soc. Am. B* **23**, 1207 (2006)
7. I.I. Novikov, L.Ya. Karachinsky, M.V. Maximov, Yu.M. Shernyakov, S.M. Kuznetsov, N.Yu. Gordeev, V.A. Shchukin, P.S. Kop'ev, N.N. Ledentsov, U. Ben-Ami, V.P. Kalosha, A. Sharon, T. Kettler, K. Posilovic, D. Bimberg, V. Mikhelashvili, G. Eisenstein, *Appl. Phys. Lett.* **88**, 231108 (2006)
8. I.I. Novikov, N.Yu. Gordeev, Yu.M. Shernyakov, Yu.Yu. Kiselev, M.V. Maximov, P.S. Kop'ev, A. Sharon, R. Duboc, D.B. Arbiv, U. Ben-Ami, V.A. Shchukin, N.N. Ledentsov, *Appl. Phys. Lett.* **92**, 103515 (2008)
9. K. Posilovic, T. Kettler, V.A. Shchukin, N.N. Ledentsov, U.W. Pohl, D. Bimberg, J. Fricke, A. Ginolas, G. Erbert, G. Tränkle, J. Jönsson, M. Weyers, *Appl. Phys. Lett.* **93**, 221102 (2008)
10. B.J. Bijlani, A.S. Helmy, *Opt. Lett.* **34**, 3734 (2009)
11. C.Z. Tong, B. Bijlani, S. Alali, A.S. Helmy, *IEEE J. Quantum Electron.* **46**, 1605 (2010)
12. P. Abolghasem, A.S. Helmy, *IEEE J. Quantum Electron.* **45**, 646 (2009)
13. P. Abolghasem, J. Han, B. Bijlani, A. Arjmand, A.S. Helmy, *IEEE Photonics Technol. Lett.* **21**, 1462 (2009)
14. V.P. Kalosha, K. Posilovic, T. Kettler, V.A. Shchukin, N.N. Ledentsov, D. Bimberg, *Semicond. Sci. Technol.* **26**, 075014 (2011)
15. H. Yoshida, T. Numai, *Jpn. J. Appl. Phys.* **49**, 012101 (2010)
16. J.P. Kim, A.M. Sarangan, *Opt. Lett.* **32**, 536 (2007)
17. J.S. Yu, S. Slivken, A.J. Evans, M. Razeghi, *IEEE J. Quantum Electron.* **44**, 747 (2006)
18. R.L. Lucke, *ArXiv Phys. E-Prints*, April 2006
19. N. Zareian, P. Abolghasem, A.S. Helmy, *J. Lightwave Technol.* **29**, 728 (2011)